Modern Pathology (2020) 33:2458–2472
https://doi.org/10.1038/s41379-020-0638-5

ARTICLE

Clinicopathologic features of kinase fusion-related thyroid carcinomas: an integrative analysis with molecular characterization

Ying-Hsia Chu[1] · Lori J. Wirth[2] · Alexander A. Farahani[1] · Vânia Nosé[1] · William C. Faquin[1] · Dora Dias-Santagata[1] · Peter M. Sadow[1]

Received: 7 July 2020 / Revised: 16 July 2020 / Accepted: 16 July 2020 / Published online: 31 July 2020

Abstract

The discovery of actionable kinase gene rearrangements has revolutionized the therapeutic landscape of thyroid carcinomas. Unsolved challenges include histopathologic recognition of targetable cases, correlation between genotypes and tumor behavior, and evolving resistance mechanisms against kinase inhibitors (KI). We present 62 kinase fusion-positive thyroid carcinomas (KFTC), including 57 papillary thyroid carcinomas (PTC), two poorly differentiated thyroid carcinomas (PDTC), two undifferentiated thyroid carcinomas (ATC), and one primary secretory carcinoma (SC), in 57 adults and 5 adolescents. Clinical records, post-operative histology, and molecular profiles were reviewed. Histologically, all KFTC showed multinodular growth with prominent intratumoral fibrosis. Lymphovascular invasion (95%), extrathyroidal extension, gross and microscopic (63%), and cervical lymph node metastasis (79%) were common. Several kinase fusions were identified: *STRN-ALK*, *EML4-ALK, AGK-BRAF*, *CUL1-BRAF*, *MKRN1-BRAF*, *SND1-BRAF*, *TTYH3-BRAF*, *EML4-MET*, *TFG-MET*, *IRF2BP2-NTRK1*, *PPL-NTRK1*, *SQSTM1-NTRK1*, *TPR-NTRK1*, *TPM3-NTRK1*, *EML4-NTRK3*, *ETV6-NTRK3, RBPMS-NTRK3*, *SQSTM1-NTRK3*, *CCDC6-RET*, *ERC1-RET*, *NCOA4-RET*, *RASAL2-RET*, *TRIM24-RET*, *TRIM27-RET*, and *CCDC30-ROS1*. Individual cases also showed copy number variants of *EGFR* and nucleotide variants and indels in p*TERT*, *TP53, PIK3R1, AKT2, TSC2, FBXW7, JAK2, MEN1, VHL, IDH1, PTCH1, GNA11, GNAQ, SMARCA4*, and *CDH1*. In addition to thyroidectomy and radioactive iodine, ten patients received multi-kinase and/or selective kinase inhibitor therapy, with 6 durable, objective responses and four with progressive disease. Among 47 cases with >6 months of follow-up (median [range]: 41 [6–480] months), persistent/recurrent disease, distant metastasis and thyroid cancer-related death occurred in 57%, 38% and 6%, respectively. In summary, KFTC encompass a spectrum of molecularly diverse tumors with overlapping clinicopathologic features and a tendency for clinical aggressiveness. Characteristic histology with multinodular growth and prominent fibrosis, particularly when there is extensive lymphovascular spread, should trigger molecular testing for gene rearrangements, either in a step-wise manner by prevalence or using a combined panel. Further, our findings provide information on molecular therapy in radioiodine-refractory thyroid carcinomas.

Introduction

Protein kinases are important signaling mediators that regulate cell survival, growth and differentiation through intricate molecular pathways. Receptor tyrosine kinases (RTK), such as ALK, RET, MET, NTRK, FGFR, and ROS1, upon binding ligands, transduce signals to the RAS/RAF/MAPK, PI3K/AKT/mTOR, and JAK-STAT pathways, whose deregulated overactivation plays a central role in human carcinogenesis. The RAS/RAF/MAPK, PI3K/AKT/mTOR, and JAK-STAT signaling cascades are composed of multiple cytoplasmic tyrosine kinases (CTK), serine/threonine kinases (S/TK), and lipid kinases [1]. The

These authors contributed equally: Ying-Hsia Chu, Lori J. Wirth

These authors jointly supervised this work: Dora Dias-Santagata, Peter M. Sadow

Supplementary information The online version of this article (https://doi.org/10.1038/s41379-020-0638-5) contains supplementary material, which is available to authorized users.

✉ Peter M. Sadow
psadow@mgh.harvard.edu

[1] Departments of Pathology, Massachusetts General Hospital and Harvard Medical School, Boston, MA 02114, USA

[2] Departments of Medicine, Massachusetts General Hospital and Harvard Medical School, Boston, MA 02114, USA

activation of most RTK requires molecular dimerization. Rearrangements of RTK-encoding genes lead to ligand-independent dimerization and are well-recognized oncogenic drivers in thyroid, lung, salivary gland, breast, kidney, colorectal, pancreatic and soft tissue malignancies [2–4]. Most fusion partners provide dimerization domains, such as the coiled coil domains in *CCDC6, NCOA4, TRIM24, TPR, PPL, CCDC30, TPM3, ERC1*, the Phox and Bem1p (PB1) interaction domains in *SQSTM1* and *TFG*, the helix-loop-helix domain in *ETV6*, the zinc finger domain in *IRF2BP2*, the WD domains in *STRN,* and *EML4*, and the RNA recognition motif of *RBPMS*, to be joined with the kinase domain of the RTK in forming fusion oncoproteins that are capable of autonomous activation [5–7]. At a much lower frequency, transforming rearrangements of downstream signaling S/TK, such as BRAF and AKT, have also been reported. *BRAF* fusions are found in 60–80% of pilocytic astrocytomas and rare lung and thyroid carcinomas [8–10]. The N-terminus autoinhibitory domain of BRAF is lost as the C-terminus kinase domain fuses with a partner sequence, leading to uncontrolled activation [8]. Recently, rare cases of ovarian, peritoneal and breast tumors have showed *AKT* fusions that remove the autoregulatory pleckstrin homology domain from the kinase domain of AKT1/2/3 [11–13]. In the thyroid gland, kinase fusion-related carcinomas are uncommon occurrences that have been most frequently noted in children and young adults, as well as post-Chernobyl radiation exposure victims. However, given a shift toward pre-operative molecular testing for treatment planning, these tumors are finding an established presence in sporadic thyroid malignancies in middle aged and elderly populations. Cases involving *ALK*, *RET*, *MET*, *NTRK1/3*, *ROS1, FGFR1,* and *BRAF* fusions have been increasingly discovered with a wide range of partner genes [10, 14–19].

As genomics-driven precision oncology has brought significant changes to thyroid cancer diagnosis and therapeutics over the past several years, one pivotal breakthrough has been the successful translation of protein kinase inhibitors (KI) into clinical therapeutic use. While earlier multi-kinase inhibitors (MKI), such as lenvatinib, sorafenib, vandetanib and cabozantinib showed efficacy in thyroid cancer, MKI therapy is associated with frequent off-target side effects. Newer, more selective agents, such as larotrectinib (anti-TRK), entrectinib (anti-ALK, ROS1, and TRK), selpercatinib, and pralsetinib (both anti-RET), have demonstrated significant efficacy with more favorable side effect profiles. Recent trials in non-medullary thyroid carcinomas (mostly PTC) have reported an objective response rate of 62% and 79% for selpercatinib and larotrectinib, respectively; a duration of response was not reached in either study due to few progress events [20–24]. Nevertheless, several challenges remain to be addressed. Firstly, immunohistochemical markers are still unavailable or yet to be fully validated for most kinase rearrangements. With costly molecular methods being the current mainstay for detecting targetable alterations, it is essential to develop a clinicopathologic case triage approach for selective genetic testing. Secondly, due to the rarity of kinase fusion-related thyroid carcinomas (KFTC), their genomic make-up and long-term clinical behavior are not well understood. Furthermore, acquired resistance to kinase inhibitors has been increasingly noted. While isolated cases have been associated with secondary mutations that cause target modifications (eg. *RET* G810S, *NTRK* G595R, *ALK* G1202R, *ROS1* G2032R) and bypass signaling [2, 25, 26], the mechanisms of acquired resistance remain obscure in many cases. There exists an ongoing need for patient-based data focused on pre- and post-KI genotype-phenotype correlation in order to tailor individualized treatment for KFTC.

In this study, we present a large, single-institutional cohort of KFTC with two main purposes: [1] to describe the cardinal clinicopathologic features of KFTC to guide diagnostic recognition and molecular testing referral, and [2] to contribute to the current literature on the genomic landscape of KFTC with correlation to clinical findings including KI therapy response.

Materials and methods

Case identification

With the approval by the Massachusetts General Hospital (MGH) institutional review board (2012P001024), we retrospectively queried the MGH molecular pathology database for primary thyroid carcinomas that underwent targeted gene rearrangement analysis (described below) from 2013 through the May of 2020, and reviewed the test results. Since 2013, the pathologists and other providers at MGH have been selectively submitting cases for genetic profiling based upon unusual histology, aggressive presentation, and/or negative BRAF V600E mutant-specific immunohistochemistry, or for clinical decision-making. For cases that showed kinase gene rearrangements, histologic slides were obtained from the MGH surgical pathology archive and reviewed by three pathologists (PMS, VN, and YHC). Patient clinical information, surgical and molecular pathology reports were accessed through the electronic medical record interface at MGH. Histologic findings, such as clear cell, oncocytic, tall cell, hobnail, and high-grade (defined as solid, trabecular, or insular pattern with necrosis and/or ≥3 mitoses per 10 high-power fields [HPF]) features, were semi-quantified as focal (<30% of sampled tumor volume) versus diffuse.

Immunohistochemistry

We recently described the immunohistochemistry (IHC) setup at MGH [27]. IHC markers that were employed in this study as needed to characterize morphologically unusual and genetically altered cases included TTF1 (performed in cases 1, 52, 53; clone 8G7G3/1; dilution 1:300; Dako, Carpinteria, CA), BRG1 (performed in case 9; clone EPR3912; dilution 1:50; Abcam, Cambridge, United Kingdom), GATA3 (performed in case 25; clone L50-823, dilution 1:200; Cell Marque, Rocklin, CA), mammaglobin (performed in case 25; clone 304-1A5; dilution 1:250; Dako, Carpinteria, CA), S100 protein (performed in case 25; polyclonal and prediluted; Ventana, Oro Valley, AZ), PAX8 (performed in cases 25, 52, 53; polyclonal, dilution 1:1000; Proteintech, Rosemont, IL), thyroglobulin (performed in cases 25, 52; dilution 1:800; Cell Marque, Rocklin, CA), E-cadherin (performed in case 46; clone 36B5; Leica Biosystems, Buffalo Grove, IL), p40 (performed in case 52; clone BC28, Biocare, Concord, MA) and BRAF V600E (performed in all cases; clone VE1; dilution 1:200; Abcam, Cambridge, United Kingdom).

Targeted gene rearrangement next-generation sequencing (NGS) analysis

An Anchored Multiplex PCR (AMP) assay developed at MGH [28] was performed for detecting targeted gene fusions by next-generation sequencing (NGS) using total nucleic acid extracted from formalin-fixed paraffin embedded (FFPE) tumor tissue. The details of the assay were as we recently described [27] and covered the following genes (exons): *ALK* (19–22, intron 19), *BRAF* (7–12, 15), *EGFR* (2–7 exon skipping/vIII variant, 7–9, 16, 20, 24, 25), *EWSR1* (4–14), *FGFR2* (2, 8–10, 17), *MAML2* (2,3), *MET* (exon 14 skipping), *NRG1* (1–3, 6), *NUTM1* (3), *RET* (8–13), *ROS1* (31–37), *AKT3* (1–3), *ARHGAP26* (2, 10–12), *AXL* (19,20), *BRAF* (7–12, 15), *BRD3* (9–12), *BRD4* (10, 11), *ERG* (2–11), *ESR1* (3–6), *ETV1* (3–13), *ETV4* (2, 4–10), *ETV5* (2, 3, 7–9), *ETV6* (1–7), *FGFR1* (2, 8–10, 17), *FGFR3* (8–10, 17, intron 17), *FGR* (2), *INSR* (12–22), *JAZF1* (2–4), *MAML2* (2,3), *MAST1* (7–9, 18–21), *MAST2* (2, 3, 5, 6), *MET* (13, 15), *MSMB* (2–4), *MUSK* (7–9, 11–14), *MYB* (7–9, 11–16), *NOTCH1* (2, 4, 26–31, internal exon 3–27 deletion), *NOTCH2* (5–7, 26–28), *NRG1* (1–3, 6), *NTRK1* (8,10–13), *NTRK2* (11–17), *NTRK3* (13–16), *NUMBL* (3), *PDGFRA* (7, exon 8 deletion, 10–14), *PDGFRB* (8–14), *PIK3CA* (2), *PKN1* (10–13), *PPARG* (1–3), *PRKCA* (4–6), *PRKCB* (3), *RAF1* (4–7, 9–12), *RELA* (3, 4), *RSPO2* (1, 2), *RSPO3* (2), *TERT* (2), *TFE3* (2–8), *TFEB* (1,2), *THADA* (28), and *TMPRSS2* (1–6). Illumina MiSeq 2 × 147 base paired-end reads were mapped to the hg19 human reference genome using BWA-MEM [29] and interpreted by a molecular pathologist (DDS).

SNaPshot mutational profiling

As previously described [30], the SNaPshot assay was AMP-based and validated for clinical application at MGH. Utilizing the ArcherDx and Illumina NextSeq platforms, the assay targeted single nucleotide variants (SNVs) and insertion/deletions (indels) in the following genes (exons): *ABL1* (4–7), *AKT1* (3,6), *ALK* (21–23,25), *APC* (16), *ARID1A* (1–20), *ATM* (1–63), *ATRX* (1–35), *AURKA* (2,5–8), *BRAF* (11,15), *BRCA1* (2–23), *BRCA2* (2–27), *CCNB1* (2,[3-partial],5,[6-partial],7), *CCND2* ([2-partial],3-4,[5-partial]), *CCND3* (2–5-partial), *CCNE1* (3–8,10,12), *CDH1* (1–16), *CDK4* (2–7), *CDK6* (6), *CDKN2A* (1–3), *CIC* (1–20), *CSF1R* (7,22), *CTNNB1* (3), *DAXX* (1–8), *DDR2* (12–18), *DDX3X* (1–17), *EGFR* (3,7,15,18–21), *ERBB2* (8,10,19–21,24), *ERBB3* (2-3,7-8), *ERBB4* (3-4,6–9,15,23), *ESR1* (8), *EZH2* (16), *FBXW7* (1–11), *FGFR1* (4,7-8,13,15,17), *FGFR2* (7,9,12,14), *FGFR3* (7–9,14–16,18), *FLT3* (11,14,16,20), *FOXL2* (1), *GNA11* (5), *GNAQ* (4-5), *GNAS* (6–9), *H3F3A* (2), *HNF1A* (3-4), *HRAS* (2-3), *IDH1* (3-4), *IDH2* (4), *JAK2* (11,13-14,16,19), *JAK3* (4,13,16), *KDR* (6-7,11,19,21,26-27,30), *KEAP1* (2–6), *KIT* (2,8–11,13–15,17-18), *KRAS* (2–5), *MAP2K1* (2,3,6-7), *MAP3K1* (1–20), *MDM2* (2–4,6,8,10), *MDM4* ([4-partial],5-6,[7,9–11-partial]), *MEN1* (2–10), *MET* (2,11,14,16,19,21), *MITF* (1-partial), *MLH1* (12), *MPL* (10), *MSH6* (1–10), *MSI*, *MYC* (1–3), *MYCN* (3), *NF1* (1–58), *NF2* (1–15), *NKX2-1* (1-partial), *NOTCH1* (25–27,34), *NPM1* (11), *NRAS* (2–5), *PDGFRA* (12,14-15,18,23), *PIK3CA* (2,5,7-8,10,14,19,21), *PIK3R1* (1–10), *POLE* (9–14), *PTCH1* (1–23), *PTEN* (1–9), *PTPN11* (3,13), *RB1* (1–27), *RET* (10-11,13–16), *RHOA* (2-3), *RNF43* (2–10), *ROS1* (36–38), *SDHB* (1–8), *SMAD2* (7), *SMAD4* (2–12), *SMARCA4* (3–36), *SMARCB1* (2,4,5,9), *SMO* (3,5-6,9,11), *SRC* (14), *STAG2* (3–34), *STK11* (1–9), *SUFU* (1–12), *TERT* (1), *TP53* (1–11), *TP63* (1–14), *TSC1* (3–23), *TSC2* (2–42), *TSHR* (10), and *VHL* (1–3). In addition, the following copy number variations (CNVs) were covered: *ABL1, AKT1, ALK, APC, ARID1A, ATM, ATRX, AURKA, BRAF, BRCA1, BRCA2, CAMTA1, CCNB1, CCND1, CCND2, CCND3, CCNE1, CDK4, CDKN2A, CDK6, CIC, CDH1, CSF1R, DAXX, DDR2, DDX3X, EGFR, ERBB2 (HER-2), ERBB3, ERBB4, FBXW7, FGF19, FGFR1, FGFR2, FGFR3, FLT3, FOXL2, GLI2, GNA11, GNAQ, GNAS, HNF1A, HRAS, IDH1, JAK2, JAK3, KDR, KEAP1, KIT, KRAS, MAP2K1, MAP3K1, MDM2, MDM4, MEN1, MET, MITF, MLH1, MSH6, MYC, MYCN, NF1, NF2, NKX2-1, NOTCH1, NRAS, PDGFRA, PIK3CA, PIK3R1, PLAUR, POLE, PTCH1, PTEN, PTPN11, RB1, RET, RHOA, RNF43, SDHB, SMAD2, SMAD4, SMARCA4,*

SMARCB1, SMO, SRC, STAG2, STK11, SUFU, TERT, TP53, TP63, TSC1, TSC2, and *VHL*. Sequencing results were interpreted by a molecular pathologist (DDS).

Results

Clinical presentation

A total of 395 primary thyroid carcinomas underwent targeted gene rearrangement panel assay from 2013 to the May of 2020, including 212 (54%) papillary thyroid carcinomas (PTC), 55 (14%) medullary thyroid carcinomas, 39 (10%) undifferentiated (anaplastic) thyroid carcinomas (ATC), 36 (9%) follicular thyroid carcinomas, 24 (6%) Hürthle cell carcinomas, 23 (6%) poorly differentiated thyroid carcinomas (PDTC), one (<1%) primary thyroid secretory carcinoma (SC) and five (1%) unclassifiable carcinomas. Various kinase fusions were detected in 62 (16%) cases, including 57 (14%) PTC (including 29 classical type, 21 diffuse sclerosing variant, four solid variant, two follicular variant, and one tall cell variant), two (<1%) PDTC, two (<1%) ATC, and one SC. The most commonly rearranged kinase gene was *RET*, positive in 31 (8%) cases, followed by *NTRK3* in 11 (3%) cases, *NTRK1* in 8 (2%) cases, *BRAF* in 6 (2%) cases, *ALK* in 3 (<1%) cases, *MET* in two cases, and *ROS1* in one case. The observed fusions and clinicopathologic characteristics of all patients are summarized in Table 1 and Fig. 1, including the references for 16 previously published cases [16, 17, 27, 28, 31].

The median (range) age for patients with KFTC was 36 (13–76) years, including 57 adults and five adolescents. The female-to-male ratio was 1.8 (40:22). Except for case 16, who received low-dose radiation therapy for acne >30 years prior to developing thyroid cancer, all other cases were radiation-naïve. Tumor size ranged from 0.2 to 10.5 cm (median 3.0 cm), staged as pT1 in 15 (24%, including five microcarcinomas), pT2 in 8 (13%), pT3 in 33 (53%) and pT4 in 5 (8%) at the time of diagnosis. T stage was unavailable for case 52, whose thyroidectomy was in 1984, and neither the original histopathologic report nor the slides were available for review. Cervical lymph node metastases were noted in 49 (79%) patients, and the lateral compartment was involved (N1b) in 36 (58%). Four patients had distant metastases to lung (cases 17, 23, 53), mediastinum (case 13) and bone (case 53) at the initial presentation.

Histologic and molecular features

As listed in Table 1, 25 different kinase fusions were found, each with a preserved kinase domain. Interestingly, all cases showed remarkably similar histologic features at low magnification. Multinodular growth was consistently observed, with dense arborizing bands of fibrosis entrapping and encircling irregular-shaped tumor nodules in a pattern somewhat reminiscent of hepatic cirrhosis (Figs. 2–6). At higher magnification, the cellular architecture varied with the underlying molecular alterations, as described below. Extrathyroidal extension was present in 39 (63%) cases, involving the strap muscle in seven (11%) cases and beyond (T4 disease) in five (8%) (Fig. 1). Lymphovascular invasion was seen in most patients (95%) except for cases 3, 10, and 49. The histopathologic and genetic findings of all the cases are summarized in Fig. 1. A list of gene transcripts based on which we annotated the observed fusions is provided in Supplementary Table S1. All the kinase fusion-related cases underwent the BRAF V600E mutant-specific immunohistochemical staining and were all negative. All the cases profiled using SNaPshot lacked the *BRAF* V600E mutation (Fig. 1).

ALK-rearranged thyroid carcinomas

ALK rearrangements were found in one PDTC (case 1) and two PTC (cases 2 and 3). The two PTC, despite having different fusion partners (*STRN* and *EML4*), were morphologically similar with multinodular growth and predominantly follicular architecture (Fig. 2a, b). Scattered papillary architecture was present in case 3 (5% of tumor volume) whereas case 2 was entirely follicular-patterned. Calcifications were seen in case 2 (mostly dystrophic with rare psammoma bodies) but not in case 3. There was no additional genetic alteration in either PTC by SNaPshot. Case 1, a PDTC harboring both a *STRN-ALK* fusion and a pathogenic *TP53* mutation c.772G>C (p.Glu258Gln), consisted of solid nests of polygonal malignant cells with admixed clear, oncocytic and squamoid features, along with frequent mitoses and necrosis (Fig. 2c, d). One 0.1 cm focus of follicular-patterned PTC was found within the tumor with abrupt transition into the predominantly poorly differentiated morphology (Fig. 2d). IHC showed diffuse TTF1 expression supporting a PDTC diagnosis.

BRAF-rearranged thyroid carcinomas

BRAF fusions were found in six PTC (cases 4–9) including two with high-grade features (cases 7 and 8). A packeted, papillary appearance was seen in cases 4, 5, 6, and 9, characterized by nodules of papillae encircled by dense fibrosis (Fig. 3a, b). The two *BRAF-SND1* fusion PTC (cases 7 and 8) were histologically unique for having admixed classical (accounting for 40% and 20% of tumor volume, respectively), tall cell (40% and 10%), solid (10% and 30%), and follicular (10% and 40%) components and focal high-grade features (up to 4 mitoses/10 HPF in case 7; focal necrosis in both cases; Fig. 3c, d). Psammomatous calcifications were numerous in case 4, rare in case 5, and absent in cases 6–9.

Table 1 Clinical characteristics of kinase fusion-related thyroid carcinomas.

Case[a]	Rearrangement	Fusion exons	Age (years)	Sex	Stage	Distant metastasis	Treatment	Followup (months)	Outcome	Ref
1	*STRN-ALK*	S3; A20	61	M	T3 N1b	Skin, mediastinum (both R)	Sorafenib, crizotinib, lenvatinib[a]	22	R; on hospice	
2	*STRN-ALK*	S3; A20	66	F	T1 N0	–	–	19	NED	
3	*EML4-ALK*	E6; A20	32	M	T1 N0	–	–	96	NED	[17]
4	*AGK-BRAF*	A2; B8	15	F	T3 N1b	Lung (R)	RAI	33	AWD	
5	*CUL1-BRAF*	C7; B9	67	M	T4a N1b	–	RAI	27	AWD	
6	*MKRN1-BRAF*	M3; B10	55	M	T1 N1a	–	RAI	5	NED	
7	*SND1-BRAF*	S14; B11	75	M	T3 N0	–	RAI	15	NED	
8	*SND1-BRAF*	S14; B9	76	F	T2 N0	–	RAI	30	NED	
9	*TTYH3-BRAF*	T12; B8	60	M	T4a N1b	–	XRT, RAI	24	NED	
10	*EML4-MET*	E6; M15	61	F	T2 N0	–	RAI	46	NED	
11	*TFG-MET*	T5; M15	44	F	T1 N0	–	–	2	NED	[17]
12	*IRF2BP2-NTRK1*	I1; N10	36	F	T1 N0	–	–	1	NED	
13	*PPL-NTRK1*	P21; N11	62	M	T3 N1b	Mediastinum (D), lung (R)	RAI, trametinib, larotrectinib[a]	80	R; AWD	[28]
14	*SQSTM1-NTRK1*	S5; N10	37	F	T2 N1a	–	RAI	44	AWD	[27]
15	*SQSTM1-NTRK1*	S5; N10	74	F	T1 N0	–	–	1	NED	
16	*TPR-NTRK1*	T20; N11	54	M	T3 N1b	Lung (R)	RAI, larotrectinib[a]	144	R x2; AWD	[27]
17	*TPR-NTRK1*	T21; N12	24	M	T3 N1b	Lung (D)	RAI	34	AWD	[27]
18	*TPM3-NTRK1*	T7; N10	40	M	T3 N1a	–	–	1	AWD	
19	*TPM3-NTRK1*	T7; N12	27	M	T3 N1b	–	–	0.2	AWD	
20	*EML4-NTRK3*	E2; N13	42	M	T3 N1b	Lung, brain (both R)	RAI, XRT, entrectinib[a]	480	R x2; AWD	[27]
21	*ETV6-NTRK3*	E3; N13	74	F	T3 N1b	–	RAI; XRT	13	R; AWD	[27]
22	*ETV6-NTRK3*	E4; N13	32	F	T3 N1b	–	RAI	39	NED	[27]
23	*ETV6-NTRK3*	E4; N13	14	F	T3 N1b	Lung (D)	RAI	80	R; AWD	[27]
24	*ETV6-NTRK3*	E5; N14	71	F	T3 N1a	–-	RAI, XRT, larotrectinib[a]	71	R x2; NED	[27]
25	*ETV6-NTRK3*	E4; N13	23	F	T1 N0	–	–	1	NED	
26	*RBPMS-NTRK3*	R5; N13	22	F	T3 N1a	–	RAI	44	NED	[27]
27	*RBPMS-NTRK3*	R5; N13	60	F	T3 N1a	Lung (R)	RAI, proton beam radiation	121	R x2; AWD	[27]
28	*SQSTM1-NTRK3*	S5; N13	43	F	T3 N1b	Lung (R)	RAI	16	AWD	[27]
29	*SQSTM1-NTRK3*	S5; N13	29	F	T1 N0	–	–	0.5	AWD	
30	*SQSTM1-NTRK3*	S5; N13	26	F	T2 N1a	–	–	1	AWD	
31	*CCDC6-RET*	C1; R12	72	M	T3 N1b	Brain, lung (both R)	RAI, SRS, doxorubicin, docetaxel, selpercatinib[a]	35	R; AWD	[31]
32	*CCDC6-RET*	C1; R12	40	F	T3 N1b	–	RAI	41	R x2; AWD	
33	*CCDC6-RET*	C1; R12	19	F	T3 N1b	–	RAI	69	R; AWD	
34	*CCDC6-RET*	C1; R12	19	F	T3 N1b	–	RAI	27	AWD	
35	*CCDC6-RET*	C1; R12	37	F	T1 N1b	–	RAI	19	R; AWD	
36	*CCDC6-RET*	C1; R12	17	F	T3 N1b	–	RAI	49	AWD	
37	*CCDC6-RET*	C1; R12	23	F	T1 N1b	–	RAI	20	R; AWD	
38	*CCDC6-RET*	C1; R12	23	F	T3 N1b	–	RAI	63	R; AWD	

Table 1 (continued)

Case[a]	Rearrangement	Fusion exons	Age (years)	Sex	Stage	Distant metastasis	Treatment	Followup (months)	Outcome	Ref
39	*CCDC6-RET*	C1; R12	26	M	T3 N1b	–	RAI	6	AWD	
40	*CCDC6-RET*	C1; R12	16	M	T2 N1b	–	RAI	2	AWD	
41	*CCDC6-RET*	C1; R12	44	M	T4a N1b	Spine, axilla (both R)	RAI, XRT, SBRT, selpercatinib[a]	136	R x2; AWD	
42	*CCDC6-RET*	C1; R12	51	M	T3 N1b	Lung (R)	RAI	47	AWD	
43	*CCDC6-RET*	C1; R12	39	F	T3 N1b	Lung (R)	RAI	41	AWD	
44	*CCDC6-RET*	C1; R12	53	M	T2 N1a	–	RAI	3	AWD	
45	*CCDC6-RET*	C1; R12	67	F	T1 N1a	–	RAI	54	NED	
46	*CCDC6-RET*	C1; R12	33	F	T1 N1a	–	RAI	6	NED	
47	*CCDC6-RET*	C1; R12	25	F	T1 N0	–	RAI	27	NED	
48	*CCDC6-RET*	C1; R12	19	F	T3 N0	–	RAI	32	NED	
49	*CCDC6-RET*	C1; R12	51	F	T2 N0	–	–	0.03	NED	
50	*CCDC6-RET*	C1; R12	21	M	T3 N1b	–	–	1	AWD	
51	*CCDC6-RET*	C1; R12	25	F	T3 N1b	–	–	1	AWD	
52	*ERC1-RET*	E7; R12	13	F	Tx N1[b]	Lung, brain, bone, breast (all R)	RAI, XRT, SRS, kinase inhibitors[a]	441	R x2; DOD	
53	*NCOA4-RET*	N8; R12	61	M	T4a N1b	Lung (D), bone (D)	Inoperable presentation; XRT, kinase inhibitors[a]	35	DOD	
54	*NCOA4-RET*	N8; R12	58	F	T2 N1b	–	RAI	3	AWD	
55	*NCOA4-RET*	N8; R12	31	M	T3 N1b	–	RAI	21	R; AWD	
56	*NCOA4-RET*	N8; R12	26	F	T3 N1b	–	RAI	63	NED	
57	*NCOA4-RET*	N7; R12	55	F	T3 N1b	–	RAI	7	NED	
58	*NCOA4-RET*	N8; R12	36	F	T1 N1b	Liver, lung, pleura, bone, abdominal wall (all R)	RAI, XRT, lenvatinib[a]	250	R x2; DOD	
59	*RASAL2-RET*	R17; R12	33	F	T1 N1a	–	RAI	61	NED	
60	*TRIM24-RET*	T10; R12	20	F	T3 N1[b]	Lung (R)	RAI	372	AWD	
61	*TRIM27-RET*	T3; R12	26	M	T3 N1b	Lung (R)	RAI	54	AWD	
62	*CCDC30-ROS1*	C10; R36	24	F	T4a N1b	–	RAI	20	NED	[16]

D at diagnosis, *na* not available, *R* recurrence, *RAI* radioactive iodine, *XRT* external radiation therapy, *SRS* stereotactic radiosurgery, *SBRT* stereotactic body radiation therapy, *AWD* alive with disease, *NED* alive with no evidence of disease, *DOD* died of disease.

[a]See Table 2 for treatment details.

[b]Thyroidectomy was performed prior to 2000 with limited staging information in the archived pathology reports, histologic slides were no longer in storage.

SNaPshot mutational profiling revealed a *TERT* pathogenic mutation c.−146C>T (C250T) in three out of the five tested (60%) patients (Fig. 1). A *TP53* in-frame deletion (p.Val218_Pro219delinsAla) was found in case 5. A *SMARCA4* mutation (p.Gly1030Ser) of unknown significance was detected in case 9, which showed retained nuclear BRG1 expression by IHC.

MET-rearranged thyroid carcinomas

EML4-MET and *TFG-MET* fusions were detected in cases 10 and 11, respectively. The two PTC were similar in having a lobulated appearance, traversing fibrosis, and predominantly follicular architecture (Fig. 4a). A papillary component was present in case 10 (20% of tumor volume; Fig. 4a, b) whereas case 11 was entirely follicular-patterned. In addition, case 11 showed diffuse clear cell change, as previously described [17].

NTRK-rearranged thyroid carcinomas (NRTC)

We recently described 11 NRTC [27], and since then seven new NRTC have been identified (cases 12, 15, 18, 19, 25, 29, 30) using our proposed morphologic approach. The new cases were all PTC and harbored fusions that included *IRF2BP2-NTRK1*, *SQSTM1-NTRK1*, *TPM3-NTRK1*, *ETV6-*

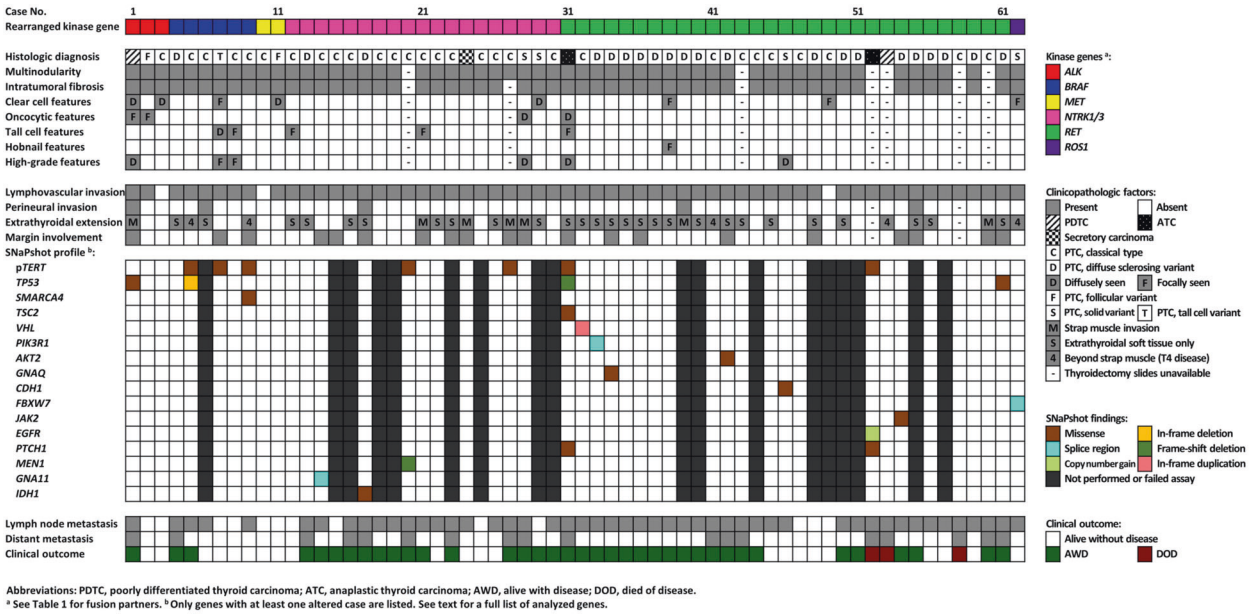

Fig. 1 Clinicopathologic and molecular features of kinase fusion-related thyroid carcinomas. This figure is a concise summary of reported MGH KFTC cases, including gene fusions, subsequent/current gene mutations, and clinical outcomes.

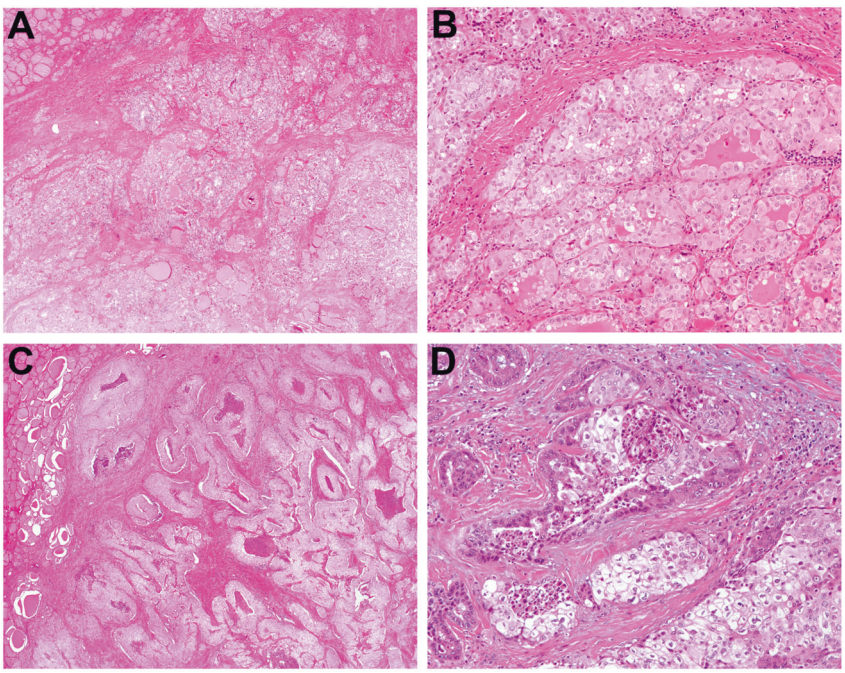

Fig. 2 *ALK*-rearranged thyroid carcinomas. Case 2, an *ALK-STRN* fusion PTC, showed multinodular growth at low magnification with traversing fibrosis (**a**). Follicular architecture was seen at high magnification (**b**). Case 1, an *ALK-STRN* fusion PDTC with a concurrent *TP53* mutation c.772G>C, consisted of numerous solid tumor nodules with comedo-type necrosis and extensive fibrosis (**c**). One 0.1 cm focus of follicular-patterned PTC was found within the tumor with abrupt transition to predominantly high-grade morphology characterized by admixed clear, oncocytic and squamoid cells and necrosis (**d**).

NTRK3, and *SQSTM1-NTRK3* (Table 1). In addition, although case 13 has been previously included in a validation study for the gene rearrangement NGS panel [28], its histopathologic features are first reported here. Overall, cases 12 (harboring *IRF2BP2-NTRK1*), 13 (*PPL- NTRK1*), and 25 (*ETV6-NTRK3*) were morphologically similar, composed of lobules of partially fused papillae with scattered glomeruloid structures and scant colloid production (Fig. 5a, b). IHC was performed in case 25 to exclude the possibility of SC phenotype and were positive for PAX8 (diffuse) and thyroglobulin (focal); S100, mammaglobin, and GATA3 were all negative. The two *TPM3-NTRK1* fusion PTC (cases 18 and 19) were both predominantly follicular-patterned with abundant colloid production and isolated foci of papillary architecture (Fig. 5c). Case 15 (*SQSTM1-NTRK1*) had a mixture of 60% follicular, 20% solid, and 20% papillary growth. The two *SQSTM1-NTRK3* fusion PTC (cases 29 and 30) were architecturally different.

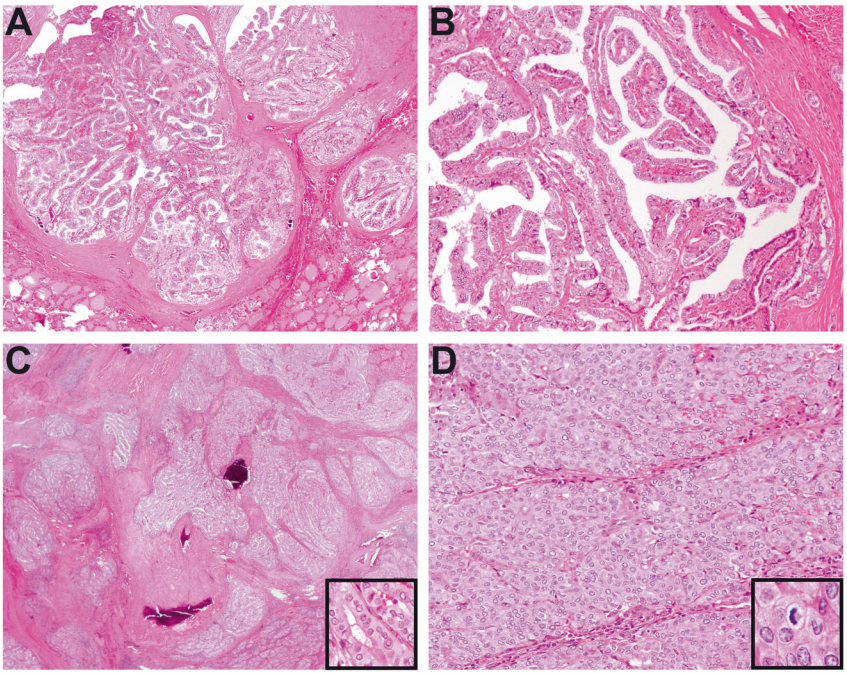

Fig. 3 *BRAF* fusion-related thyroid carcinomas. Case 5, despite having additional *TP53* and *TERT* promoter mutations, was histologically similar to cases 4, 6, and 9, consisting of multiple nodules of well-formed papillae encircled by dense fibrosis (**a**, **b**). Case 7, an *SND1-BRAF* fusion tall cell variant of PTC, showed extensive fibrosis that divided neoplastic cells into irregularly shaped islands (**c**, inset showing tall cell features). In approximately 10% of the tumor volume, a solid to trabecular architecture was noted along with increased mitotic activity (up to 4 mitoses per 10 high-power fields, inset) and focal necrosis (**d**).

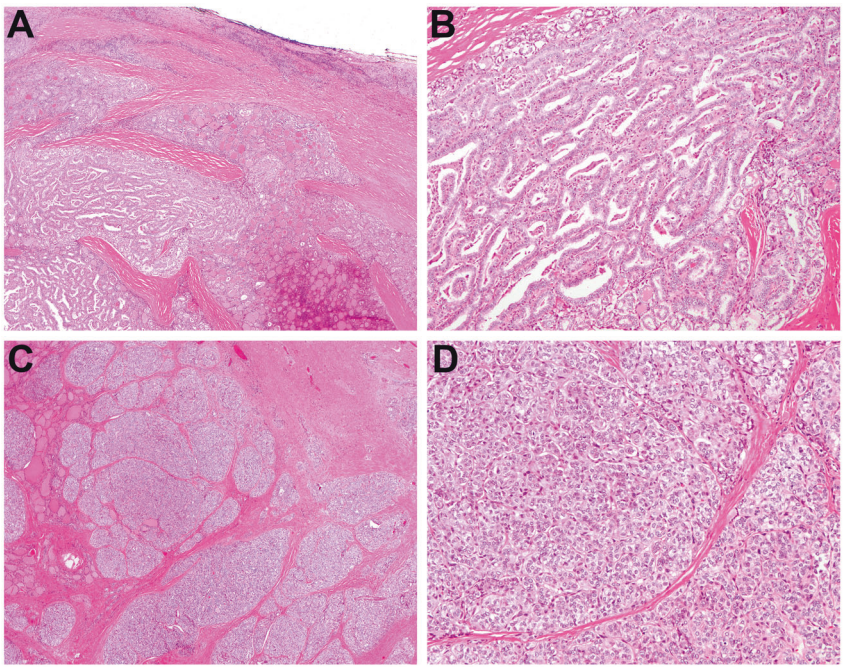

Fig. 4 *MET*-rearranged thyroid carcinoma. Case 10, an *EML4-MET* fusion PTC, was characterized by a lobulated appearance, traversing fibrosis, and predominantly follicular architecture with a minor papillary component (around 20% of tumor volume) (**a**, **b**). Case 62, a *CCDC30-ROS1* fusion PTC, was composed of numerous solid nodules of pale to clear tumor cells with arborizing fibrosis (**c**, **d**).

Case 29 was entirely solid with scattered microfollicles (Fig. 5d), whereas case 30 was entirely papillary. Psammomatous calcifications were seen in all the cases except for case 29.

RET-rearranged thyroid carcinomas

RET fusions were detected in 28 PTC, one PDTC, and two ATC. As summarized in Fig. 1, most *RET*-rearranged PTC were morphologically similar, composed of nodules of crowded papillae with a minor follicular component and arborizing sclerosis (Fig. 6a). The majority also showed squamous metaplasia, lymphocytic infiltration, and extensive lymphovascular spread of tumor cells and numerous psammoma bodies throughout the thyroid, thus fulfilling the defining features of the so-called diffuse sclerosing variant (Fig. 6a, b). Nine other cases had fewer psammoma bodies and lacked squamous metaplasia and were hence

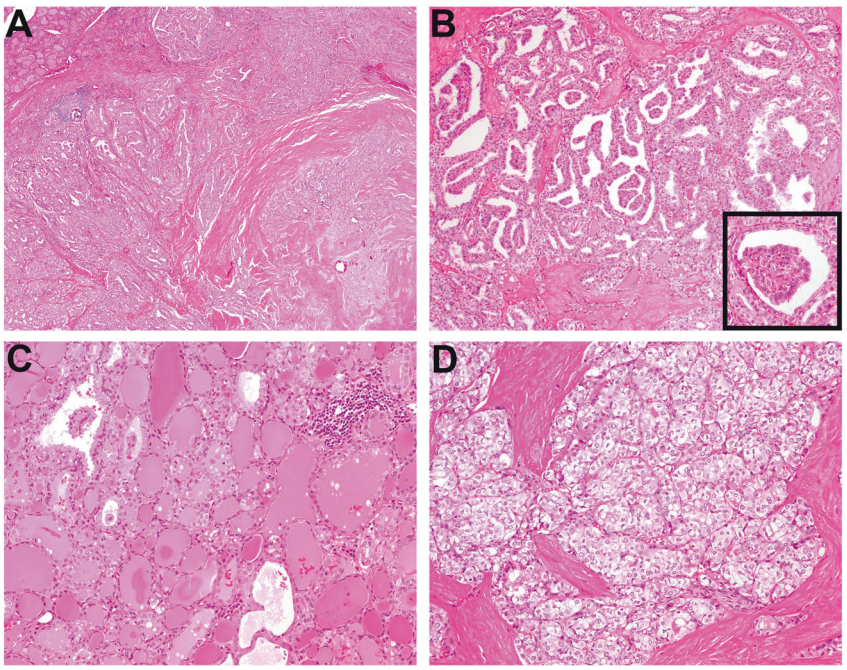

Fig. 5 *NTRK*-rearranged thyroid carcinomas. Case 12, an *IRF2BP2-NTRK1* fusion PTC, was composed of lobules of partially fused papillae with scant colloid production (**a**) and scattered glomeruloid structures and (**b**). Case 18, a *TPM3-NTRK1* fusion PTC, was predominantly follicular-patterned with abundant colloid production and isolated foci of papillary formation (**c**). Case 29, an *SQSTM1-NTRK3* fusion PTC demonstrated solid architecture with scattered microfollicles and prominent streaming fibrosis (**d**).

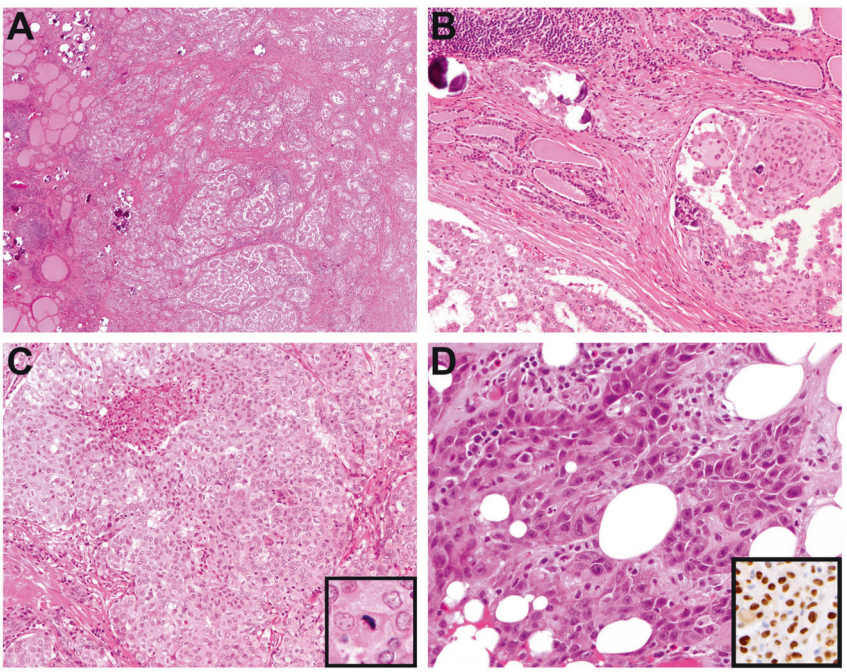

Fig. 6 RET fusion-related thyroid carcinomas. Case 51, a *CCDC6-RET* fusion PTC, showed numerous cellular nodules and stromal sclerosis (**a**). Frequent, variably-sized psammoma bodies and tumor nests with squamous morular metaplasia were seen scattered within background thyroid (**a**, **b**). Case 46, a *CCDC6-RET* fusion PTC with concurrent *CDH1* mutation, showed a solid architecture with up to three mitoses per 10 high-power fields and focal necrosis (**c**). Case 52, after a long-standing history of PTC since childhood, showed anaplastic transformation in the scapular metastatic tumor. The cells displayed moderate pleomorphism, frequent mitoses, and squamoid cytology (**d**). PAX8 was diffusely positive (**d**, inset).

categorized as classical PTC. Case 46 was unique as a solid variant PTC with focal high-grade features (3 mitoses/10 HPF and focal necrosis; Fig. 6c). Several mutations of uncertain significance were found in *RET*-rearranged PTC, including an in-frame duplication within *VHL* (p.Ser43_-Glu47dup; case 32), a *PIK3R1* splice site variant (c.1020G>A; case 33), and missense mutations in *GNAQ* (p.Arg166His; case 34), *AKT2* (p.Asp151Glu; case 42), *CDH1* (p.Asp334Glu in case 46, with retained membranous E-cadherin expression by IHC), *JAK2* (p.Met88Thr; case 54), and *TP53* (p.Val31Ile; case 61).

The only *RET*-rearranged PDTC was case 53, which presented as a mostly intra-mediastinal mass extending from the left inferior thyroid. The mass remained subclinical until extensive intrathoracic metastatic disease caused hoarseness due to recurrent laryngeal nerve involvement. Given the unresectable presentation, the patient underwent a core biopsy that showed monotonous malignant cells

diffusely expressing TTF1 and PAX8. SNaPshot did not reveal additional genetic changes.

The two *RET*-rearranged ATC were cases 31 and 52. The histology and genetic abnormalities of case 31 were previously reported [31] with recent clinical progress updated in Table 2. Case 52 initially presented as a childhood PTC in 1984, which, after two recurrences in 1998 and 2012, exhibited accelerated progression in 2013 with widespread metastases to the sternum, scapula, brain, lung, and breast. Resections of sternal and scapular metastases showed high-grade carcinoma with squamous differentiation (Fig. 6d). There was diffuse expression of PAX8 (Fig. 6d, inset) and p40 but TTF1 and thyroglobulin were lacking. The initial molecular characterization performed in a sample of post-radiation sternal metastatic tumor revealed a *ERC1-RET* fusion, a *PTCH1* mutation of uncertain pathogenicity (p.His739Phe), a *TERT* promoter mutation c.−124C>T (C228T), and an *NF2* deletion/insertions (delins) (p.GluLeuGluArgArgLeuLeuGln355TerLeuGluArgArgLeuLeuHis). After progressing on lenvatinib and selpercatinib therapy, re-profiling of her intrapulmonary tumor showed the same *RET* fusion as well as p*TERT* and *PTCH1* mutations but the *NF2* deletion was no longer detected. In addition, a copy number gain of *EGFR* was newly identified.

ROS1-rearranged thyroid carcinomas

A *CCDC30-ROS1* fusion was observed in a young adult with a solid variant PTC (case 62), which had a prior case report at the time of diagnosis in 2016 [16]. Briefly, the 3.5 cm tumor was composed of numerous oval solid nodules of pale to clear cells encircled by branching collagenous bundles (Fig. 4c, d). SNaPshot revealed an *FBXW7* splice acceptor variant (c.585-5T>A). The patient was subsequently followed for 20 months as presented below.

Treatment and outcome

All patients except for case 53 had total thyroidectomy, and most received adjuvant radioactive iodine (RAI)(Table 1). We evaluated patients for response to RAI; 32 out of 62 did not have adequate follow-up information or received RAI in the adjuvant setting, and their response was thus not evaluable. Among the 30 patients with evaluable data, there were 26 showing evidence of refractoriness based on the 2015 American Thyroid Association guidelines [32], whereas four patients were responsive (Supplementary Table S2). Overall, among the 47 KFTC cases with at least 6 months of follow-up (median [range]: 41 [6–480] months), 20 (43%) patients had no evidence of recurrent disease, despite 10 of them having presented with nodal metastasis. The other 27 (57%) patients had persistent or recurrent disease and 18 (38%) developed distant metastases. The distant metastatic rate appeared to be the highest in *NTRK*-rearranged thyroid carcinomas (7 out of 12 cases [58%] with >6 months follow-up), followed by *RET*-rearranged thyroid carcinomas (9/25, 36%), *ALK*-rearranged thyroid carcinomas (1/3, 33%), and *BRAF*-rearranged thyroid carcinomas (1/5, 20%). All *MET*- or *ROS1*-rearranged cases remained free of locoregional and distant metastatic disease at last follow-up. Three (6%) patients eventually died of advanced *RET*-rearranged thyroid carcinomas (cases 52, 53, and 58), while mortality was not noted in patients with tumors driven by other kinases. When only PTC cases were considered, a total of 42 PTC cases had >6 months of follow-up (median [range]: 41 [6 to 480] months); persistent/recurrent disease, distant metastasis, and thyroid cancer-related death was noted in 59% (25/42), 33% (14/42), and 2% (1/42) of PTC, respectively, at the last follow-up (Table 1, Fig. 1). Multi-kinase and/or selective kinase inhibitors were prescribed to ten patients, and their treatment history, response, and toxicity profiles are summarized in Table 2.

Discussion

Targeted KI play a prominent role in the modern advancement of oncologic care. Their successful application has proven highly efficacious in patients with advanced cancers who had previously been deemed to be terminal. KI also represent a substantial cause of healthcare expenditure, and the importance of laboratory guidance, both histologic and molecular, in identifying targetable cases cannot be overstated. In this study, we pointed out a characteristic and reproducible histologic pattern of KFTC. The triad of multinodularity, prominent fibrosis, and lymphovascular invasion were seen in 95% of the cases, and the former two features were present in 100% of our cohort, which encompassed PTC, SC, PDTC, and ATC driven by a wide range of kinase fusions involving *ALK*, *BRAF*, *MET*, *NTRK1/3*, *RET,* and *ROS1*. In addition, we also observed high percentages of extrathyroidal extension, micro and macroscopic (63%), lymph node involvement, central and lateral neck (79%), and distant metastasis (38%). Of note, our cohort was mostly radiation-naïve adults, whereas most of the existing KFTC literature had been conducted in pediatric and radiation-associated patients. Recently, Prasad et al. reported similar histologic findings of multinodularity, scar-like fibrosis and frequent lymphovascular spread in pediatric *NTRK*-rearranged thyroid carcinomas [33]. In another study, Pekova et al. examined 52 pediatric KFTC carrying *RET*, *NTRK1/3*, *ALK*, *BRAF,* and *MET* fusions and noted frequent multifocality (53.8%), extrathyroidal extension (40.9%), and lymph node metastasis (62.4%). Elevated metastatic rates have also been reported by other researchers

Table 2 Treatment history of patients receiving kinase inhibitor (KI) therapy.

Case #, diagnosis	Pre-KI management	Kinase inhibitor therapy and response[a]			Toxicity (grade[b])
		First regimen	Second regimen	Third regimen	
1, PDTC	T, **M** (*STRN-ALK* fusion, TP53 c.772G>C)	**Sorafenib** 400 mg BID, stopped after 19 days due to ischemic stroke.	**Crizotinib** 250 mg BID, stopped after 11 months due to PD. The BOR was SD.	**Lenvatinib** 14 mg daily while on hospice, stopped after 1 month for lethargy.	**Crizotinib**: fatigue (1). **Lenvatinib**: small oral ulcers.
13, PTC	T, RAI, **M** (*PPL-NTRK1* fusion)	**Trametinib** 2 mg daily (redifferentiation therapy) for 30 days, followed by RAI; restaging imaging showed PD.	**Larotrectinib*** 100 mg BID; CR after 10 cycles; now 45 cycles into therapy with ongoing CR.	–	**Trametinib:** fatigue (1), dysphagia (1), acneiform eruption (3). **Larotrectinib:** fatigue (1), muscle cramping (1), dysgeusia (1).
16, PTC	T, RAI, revision neck dissection, **M** (*TPR-NTRK1* fusion)	**Larotrectinib*** 100 mg BID; now on cycle 21 with ongoing PR (33% decrease).	–	–	Fatigue (1), joint pain (1); transaminitis (1).
20, PTC	T, RAI, resection and irradiation of brain metastasis, **M** (*EML4-NTRK1* fusion; *pTERT* c. −124C>T; *MEN1* frameshift deletion)	**Entrectinib**** 400 mg daily; now on cycle 38 with ongoing PR (69% decrease).	–	–	Orthostatic hypotension (3), gait disturbance (2), exertional dyspnea (1), fatigue (1), anemia (2), leukopenia (1), serum creatinine elevation (1).
24, SC	T, RAI, irradiation of cervical recurrence; **M** (*ETV6-NTRK3* fusion)	**Larotrectinib*** 100 mg BID; now on cycle 29 with ongoing PR (100% decrease of measurable tumor and undetectable thyro-globulin, but deemed PR due to small persistent lung lesions likely granulomata).	–	–	Instability (1), hypophosphatemia (1).
31, ATC	T, RAI, radiosurgery of brain metastasis, one cycle of Adriamycin/Taxotere; **M** (*CCDC6-RET*, p*TERT, TP53, TSC2, PTCH1* mutations)	**Selpercatinib***** 160 mg BID; now on cycle 28 with ongoing PR (64% decrease).	–	–	Bowel edema (1).
41, PTC	T, RAI, resection and irradiation of paraspinal metastasis, **M** (*CCDC6-RET* fusion)	**Selpercatinib***** 160 mg BID; now on cycle 18 with ongoing PR (61% decrease).	–	–	Hypertension (1).
52, ATC	T, RAI, resection and irradiation of metastases, **M** (*ERC1-RET* fusion; p*TERT*, *PTCH1* and *NF2* mutations)	**Lenvatinib** 14 mg daily, with a BOR of SD, stopped after 20 months of treatment due to PD.	**Selpercatinib***** 160 mg BID, stopped due to PD after 22 cycles (21 months). The BOR was PR (63% decrease). **Posttreatment M:** new *EGFR* copy number gain.	**Cabozantinib** 40 mg daily for 3 months followed by 60 mg daily for one month, then stopped due to wound infection; restaging imaging showed PD. **Pembrolizumab** was subsequently started one month prior to death.	**Lenvatinib**: hand-foot syndrome (1); transaminitis (1), hyperbilirubinemia (2). **Selpercatinib**: fatigue (1), transaminitis (1), hypertension (1), thrombocytopenia (1). **Cabozantinib**: transaminitis (2).
53, PDTC	Radiotherapy; **M** (*NCOA4-RET* fusion).	**Lenvatinib** 24 mg daily, stopped after five months due to PD.	**Selpercatinib***** 60–80 mg BID for 8 cycles, followed by 160 mg BID for 10 cycles and then stopped due to PD. The BOR was PR (72% decrease).	**Cabozantinib** 40 mg daily for 6 months, then combined with **pembrolizumab** for 2 months before patient died of advanced disease.	**Lenvatinib**: fatigue (1). **Selpercatinib**: diarrhea (1), transaminitis (3). **Cabozantinib**: diarrhea (2), mucositis (1).
58, PTC	T, RAI, radiotherapy, **M** (*NCOA4-RET* fusion)	**Lenvatinib** 24 mg daily; PD leading to death 8 months after treatment initiation.	–	–	None documented.

ClinicalTrials.gov identifiers: *NCT02576431; **NCT02568267; ***NCT03157128.

T thyroidectomy, *M* molecular profiling of tumor (see text for alteration details), *BID* twice daily, *RAI* radioactive iodine, *BOR* best overall response, *SD* stable disease, *PD* progressive disease, *CR* complete response, *PR* partial response, *PTC* papillary thyroid carcinoma, *PDTC* poorly differentiated thyroid carcinoma, *SC* secretory carcinoma, *ATC* anaplastic thyroid carcinoma.

[a]Response was evaluated based on the Response Evaluation Criteria In Solid Tumors (RECIST) criteria version 1.1.

[b]Based on the National Cancer Institute Common Terminology Criteria for Adverse Events (CTCAE) version 4.03.

in postradiation and sporadic thyroid carcinomas driven by *RET* [34–36], *BRAF* [37], *NTRK* [38], and *ALK* [39, 40] fusions. Although our *MET* fusion cases were non-metastatic, one of the only two previously published *MET*-rearranged PTC [15, 41] had lymph node and pulmonary metastases. Both case 62 and the only other known case of *ROS1*-rearranged thyroid carcinoma were metastatic [42]. Overall, KFTC appeared to form a group of clinically aggressive tumors with overlapping clinicopathologic characteristics which can serve as helpful clues for pathologists to initiate molecular testing. An algorithmic approach for identifying actionable kinase fusions in thyroid carcinomas is proposed in Fig. 7.

The histologic concept of "diffuse sclerosing variant (DSV)" of PTC has been commonly associated with *RET* rearrangements in the literature [43, 44]. Rendering a DSV diagnosis can be somewhat subjective, but the main defining features include extensive lymphovascular involvement, stromal sclerosis, prominent lymphocytosis, squamous metaplasia, and numerous psammoma bodies. Although the former two features were present in the vast majority of our KFTC cohort regardless of fusion type, we saw squamous

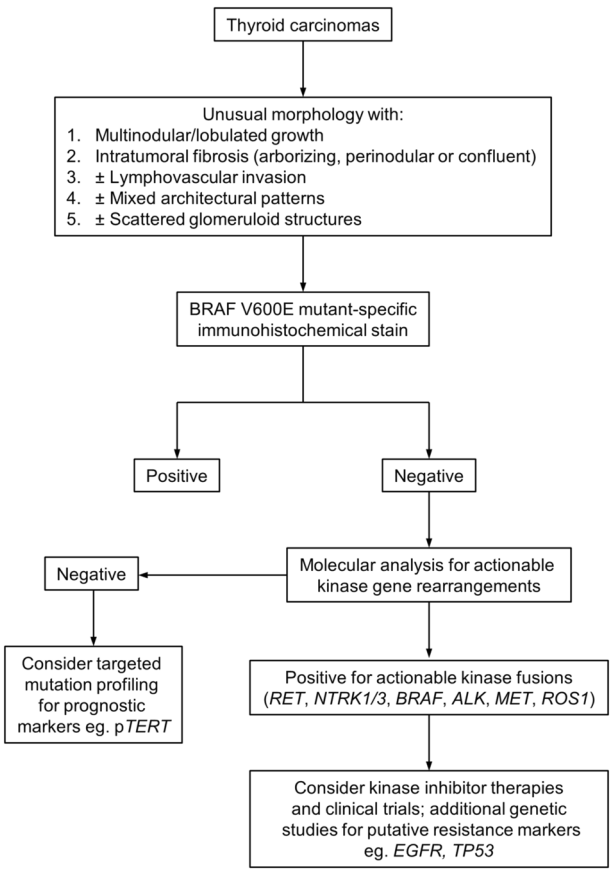

Fig. 7 Proposed algorithmic approach for identifying actionable kinase gene fusions in thyroid carcinomas. This simple algorithm provides a stepwise assessment for when further workup of thyroid carcinoma cases may yield therapeutically targetable gene fusions.

morule formation exclusively in the *RET* fusion cases. Moreover, while most of our *RET* fusion tumors showed countless psammoma bodies, cases driven by other kinases had few or none with rare exceptions (cases 4, 13, 16, 17). As a result, among a total of 21 DSV PTC in our cohort, 18 (86%) were associated with *RET* fusions, while *NTRK1* and *BRAF* fusions were implicated in two (10%) and one (5%) case, respectively. Previously, Joung et al., in examining 37 DSV PTC, reported *BRAF* V600E mutation in 24% [44]. Taken together, one plausible approach for identifying therapeutic targets in DSV cases may include immunohistochemical staining for *BRAF* V600E mutation, followed by molecular testing for *RET, NTRK,* and *BRAF* rearrangements if negative. Another histologic type that is historically associated with *RET* fusions is the solid variant PTC, which was also seen in *NTRK*- and *ROS1*-rearranged PTC in our cohort (Fig. 1).

Although previous studies have suggested that *CCDC6-RET* fusion PTC were generally indolent with a low propensity for high grade transformation [45], cases 31 (a *CCDC6-RET* fusion ATC) and 46 (a *CCDC6-RET* fusion PTC with high-grade features) exemplified the dedifferentiating potential of these tumors. It was noteworthy that both cases had genetic co-alterations. In addition to the *CCDC6-RET* fusion, case 46 also carried a *CDH1* missense variant of uncertain pathogenicity. We performed immunohistochemistry and noticed retained membranous E-cadherin staining. Nevertheless, it has been documented in the literature that aberrant E-cadherin expression can occasionally occur with carcinogenic *CDH1* mutations [46]. Case 46 had four co-occurring mutations involving *TP53, TERT* promoter, *TSC2,* and *PTCH1* [31]. We also noted various degree of high-grade features in other *RET* fusion partners (cases 52 and 53) as well as *ALK*, *BRAF*, and *NTRK*-rearranged tumors (cases 1, 7, 8, and 28; Fig. 1). The average number of co-altered genes were 3.50, 0.50, and 0.50 and 0.45 per case for ATC, PDTC, PTC with high-grade features, and PTC without high-grade features, respectively (Fig. 1). The increasing number of co-alterations accompanied by higher histologic grade supports a significant role for mutation accumulation in escalating the biological potential of KFTC. Previous genomic studies in *RET, ALK, BRAF,* and *NTRK* fusion-related ATC and PDTC using larger sequencing panels have reported similar mutation burdens involving a similar set of genes, such as *TP53*, p*TERT*, and *SMARCA4* [47–49]. It should be noted that we performed molecular analysis only in tumor tissue samples without paired normal tissue testing. Therefore, we cannot exclude the possibility that some of the detected variants, particularly those that lack clear pathogenicity data in the literature, may represent rare germline variants.

We were particularly interested in correlating genetic abnormalities with patient response to kinase inhibitor

therapy. As summarized in Table 2, four cases exhibiting kinase inhibitor resistance were encountered (cases 1, 52, 53, and 58). Case 1 was found harboring both a *STRN-ALK* fusion and *TP53* c.772G>C mutation before starting crizotinib treatment. His tumor burden initially appeared to stabilize but progressed within a year. *STRN-ALK* fusion thyroid and lung carcinomas, although rare, have been putatively sensitive to crizotinib based on a total of three case reports and one in vitro study [39, 40, 50, 51]. Although no prior study has examined the drug sensitivity of *TP53*-mutant *STRN-ALK* fusion tumors, Kron et al. have recently demonstrated that concurrent *TP53* mutations represent a significant unfavorable outcome predictor in *ALK*-rearranged lung cancer patients in all the analyzed treatment subgroups (crizotinib, next-generation ALK inhibitors, chemotherapy) [52]. Several other studies have also associated *TP53* mutations with poor crizotinib response [53–55]. Cases 52, 53 and 58 initially received lenvatinib, a repurposed VEGFR inhibitor with suboptimal efficacy against *RET*-driven tumors [2], and experienced disease progression. Cases 52 and 53 were subsequently treated with selpercatinib. Interestingly, both patients had been showing clear response (63% and 72% reduction of tumor burden) for longer than a year before developing resistance (Table 2). Posttreatment tumor genetic profiling was performed in case 52 and revealed a new copy number gain of *EGFR*, which had been absent in the pretreatment sample. Activation of bypass signaling is a well-recognized mechanism for kinase inhibitor resistance [2]. Although secondary *EGFR* gain has not been previously reported in selpercatinib-treated patients, EGFR is a well-established mediator of acquired resistance to kinase inhibitor therapy in *ALK, RET*, and *ROS1* fusion-driven lung cancers [56–59]. The mechanism of acquired resistance in case 53 was unclear since no posttreatment molecular profiling was performed. It was noteworthy that several co-alterations were found in patients with durable response to kinase inhibitors, such as *pTERT* c.−124C>T (cases 20 and 31), *MEN1* p.Pro55LeufsTer64 (case 20) [27], *TP53* p.Pro152TrpfsTer10 (case 31), *PTCH1* (p.Ala4Thr, case 31), and *TSC2* (p.Gly1356Ser, case 31) [31].

BRAF fusions occur in around 1–2% of thyroid carcinomas, mainly PTC, with a largely uncharacterized prognosis [60, 61]. The frequency is higher in pilocytic astrocytoma (60–80%), cutaneous Spitzoid melanomas (75%), and pancreatic acinar cell carcinomas (20%) [61–63]. The clinical management of *BRAF* fusion-driven tumors represents an active area of research that currently has very limited patient data. Isolated case studies in astrocytoma and melanoma have showed highly variable patient response to RAF and MEK inhibitors [64, 65]. Most interestingly, one recent study using patient-derived melanoma cells expressing *BRAF* fusion transcripts have found the sensitivity to RAF inhibitors dependent on whether the 5′ end fusion partner contributes additional dimerization domain(s). Partner-derived dimerization domains cause conformation change-mediated paradoxical activation of MAPK pathway and accelerated tumor growth when treated with first and second generation RAF inhibitors [66]. Although *BRAF* fusions with (e.g., *AKAP9-BRAF*) and without (eg. *AGK-BRAF, CUL1-BRAF*) partner-derived dimerization domains have both been discovered in thyroid carcinomas [14, 15, 67], none of the fusion partners in our cases have a known dimerization domain. Since our cases did not receive kinase inhibitor therapy, their sensitivity cannot be determined. Nevertheless, compared to the *NTRK* and *RET* fusion cases, *BRAF* fusion tumors appeared to have a better prognosis in our cohort, with the majority achieving remission after thyroidectomy and RAI treatment (Fig. 1). Additional clinical research is needed to elucidate the behavior of *BRAF* fusion-driven thyroid carcinomas and the therapeutic utility of MAPK pathway inhibitors.

In summary, our findings highlight a unique histologic pattern shared by a wide morphologic (PTC, SC, PDTC, and ATC) and molecular (*RET*, *NTRK*, *BRAF, ALK*, *MET*, and *ROS1* driven) spectrum of KFTC. The triad of multinodularity, intratumoral fibrosis, and lymphovascular involvement can serve as a helpful diagnostic aid for pathologists' recognition of these clinically aggressive but highly treatable tumors. In addition, we uncovered multiple genetic co-alterations in KFTC, which demonstrated significant consequence to patient response to targeted kinase inhibitor therapy. The study had several limitations, including a lack of paired normal tissue genetic testing and possible selection bias resulting from preferential sequencing of clinically aggressive cases. Nevertheless, we expect these data to contribute to the current understanding of KFTC with anticipated benefit for patients.

Compliance with ethical standards

Conflict of interest LJW received support from Loxo Oncology, Inc. and Genentech USA, Inc. for costs of the clinical trials listed in the footnotes of Table 2. All the other authors declare no conflict of interest.

Publisher's note Springer Nature remains neutral with regard to jurisdictional claims in published maps and institutional affiliations.

References

1. Bhullar KS, Lagarón NO, McGowan EM, Parmar I, Jha A, Hubbard BP, et al. Kinase-targeted cancer therapies: progress, challenges and future directions. Mol Cancer. 2018;17:48.
2. Subbiah V, Cote GJ. Advances in targeting RET-dependent cancers. Cancer Discov. 2020;10:498–505.
3. Kuroda N, Trpkov K, Gao Y, Tretiakova M, Liu YJ, Ulamec M, et al. ALK rearranged renal cell carcinoma (ALK-RCC): a multi-institutional study of twelve cases with identification of novel

partner genes CLIP1, KIF5B and KIAA1217. Mod Pathol. 2020. https://doi.org/10.1038/s41379-020-0578-0.
4. Gao Q, Liang WW, Foltz SM, Mutharasu G, Jayasinghe RG, Cao S, et al. Driver fusions and their implications in the development and treatment of human cancers. Cell Rep. 2018;23:227–38.e3.
5. Wai DH, Knezevich SR, Lucas T, Jansen B, Kay RJ, Sorensen PH. The ETV6-NTRK3 gene fusion encodes a chimeric protein tyrosine kinase that transforms NIH3T3 cells. Oncogene. 2000;19:906–15.
6. Farago AF, Taylor MS, Doebele RC, Zhu VW, Kummar S, Spira AI, et al. Clinicopathologic features of non-small-cell lung cancer harboring an NTRK gene fusion. JCO Precis Oncol. 2018;2018. https://doi.org/10.1200/PO.18.00037.
7. Cocco E, Scaltriti M, Drilon A. NTRK fusion-positive cancers and TRK inhibitor therapy. Nat Rev Clin Oncol. 2018;15:731–47.
8. Shin CH, Grossmann AH, Holmen SL, Robinson JP. The BRAF kinase domain promotes the development of gliomas in vivo. Genes Cancer. 2015;6:9–18.
9. Vojnic M, Kubota D, Kurzatkowski C, Offin M, Suzawa K, Benayed R, et al. Acquired BRAF rearrangements induce secondary resistance to EGFR therapy in EGFR-mutated lung cancers. J Thorac Oncol. 2019;14:802–15.
10. Ricarte-Filho JC, Li S, Garcia-Rendueles ME, Montero-Conde C, Voza F, Knauf JA, et al. Identification of kinase fusion oncogenes in post-Chernobyl radiation-induced thyroid cancers. J Clin Investig. 2013;123:4935–44.
11. Slotkin EK, Diolaiti D, Shukla NN, Dela Cruz FS, Clark JJ, Gundem G, et al. Patient-driven discovery, therapeutic targeting, and post-clinical validation of a novel AKT1 fusion-driven cancer. Cancer Discov. 2019;9:605–16.
12. Kannan K, Coarfa C, Chao PW, Luo L, Wang Y, Brinegar AE, et al. Recurrent BCAM-AKT2 fusion gene leads to a constitutively activated AKT2 fusion kinase in high-grade serous ovarian carcinoma. Proc Natl Acad Sci USA. 2015;112:E1272–7.
13. Matissek KJ, Onozato ML, Sun S, Zheng Z, Schultz A, Lee J, et al. Expressed gene fusions as frequent drivers of poor outcomes in hormone receptor-positive breast cancer. Cancer Discov. 2018;8:336–53.
14. Cordioli MI, Moraes L, Bastos AU, Besson P, Alves MT, Delcelo R, et al. Fusion oncogenes are the main genetic events found in sporadic papillary thyroid carcinomas from children. Thyroid. 2017;27:182–8.
15. Pekova B, Sykorova V, Dvorakova S, Vaclavikova E, Moravcova J, Katra R, et al. RET, NTRK, ALK, BRAF and MET fusions in a large cohort of pediatric papillary thyroid carcinomas. Thyroid. 2020. https://doi.org/10.1089/thy.2019.0802. [published online ahead of print, 2020 Jul 1].
16. Ritterhouse LL, Wirth LJ, Randolph GW, Sadow PM, Ross DS, Liddy W, et al. ROS1 rearrangement in thyroid cancer. Thyroid. 2016;26:794–7.
17. Cipriani NA, Agarwal S, Dias-Santagata D, Faquin WC, Sadow PM. Clear cell change in thyroid carcinoma: a clinicopathologic and molecular study with identification of variable genetic anomalies. Thyroid. 2017;27:819–24.
18. Okamura R, Boichard A, Kato S, Sicklick JK, Bazhenova L, Kurzrock R. Analysis of NTRK alterations in pan-cancer adult and pediatric malignancies: implications for NTRK-targeted therapeutics. JCO Precis Oncol. 2018;2018. https://doi.org/10.1200/PO.18.00183.
19. Liang J, Cai W, Feng D, Teng H, Mao F, Jiang Y, et al. Genetic landscape of papillary thyroid carcinoma in the Chinese population. J Pathol. 2018;244:215–26.
20. Hong DS, DuBois SG, Kummar S, Farago AF, Albert CM, Rohrberg KS, et al. Larotrectinib in patients with TRK fusion-positive solid tumours: a pooled analysis of three phase 1/2 clinical trials. Lancet Oncol. 2020;21:531–40.
21. Wirth LJ, Sherman E, Drilon A, Solomon B, Robinson B, Lorch J, et al. Registrational results of LOXO-292 in patients with RET-altered thyroid cancers. In: Proceedings of European Society for Medical Oncology 2019 Congress.
22. Shah MH, Sherman EJ, Robinson B, Solomon BJ, Kang H, Lorch JH, et al. Selpercatinib (LOXO-292) in patients with RET-mutant medullary thyroid cancer. J Clin Oncol. 2020;38:3594.
23. Subbiah V, Hu MI-N, Gainor JF, Mansfield AS, Alonso G, Taylor MH, et al. Clinical activity of the RET inhibitor pralsetinib (BLU-667) in patients with RET fusion+ solid tumors. J Clin Oncol. 2020;38:109.
24. Drilon A, Siena S, Ou SI, Patel M, Ahn MJ, Lee J, et al. Safety and antitumor activity of the multitargeted Pan-TRK, ROS1, and ALK inhibitor entrectinib: combined results from two phase i trials (ALKA-372-001 and STARTRK-1). Cancer Discov. 2017;7:400–9.
25. Drilon A, Nagasubramanian R, Blake JF, Ku N, Tuch BB, Ebata K, et al. A next-generation TRK kinase inhibitor overcomes acquired resistance to prior TRK kinase inhibition in patients with TRK fusion-positive solid tumors. Cancer Discov. 2017;7:963–72.
26. Cocco E, Schram AM, Kulick A, Misale S, Won HH, Yaeger R, et al. Resistance to TRK inhibition mediated by convergent MAPK pathway activation. Nat Med. 2019;25:1422–7.
27. Chu YH, Dias-Santagata D, Farahani AA, Boyraz B, Faquin WC, Nosé V, et al. Clinicopathologic and molecular characterization of NTRK-rearranged thyroid carcinoma (NRTC). Mod Pathol. 2020. https://doi.org/10.1038/s41379-020-0574-4. [published online ahead of print, 2020 May 26].
28. Zheng Z, Liebers M, Zhelyazkova B, Cao Y, Panditi D, Lynch KD, et al. Anchored multiplex PCR for targeted next-generation sequencing. Nat Med. 2014;20:1479–84.
29. Li H, Durbin R. Fast and accurate short read alignment with Burrows-Wheeler transform. Bioinformatics. 2009;25:1754–60.
30. Dias-Santagata D, Akhavanfard S, David SS, Vernovsky K, Kuhlmann G, Boisvert SL, et al. Rapid targeted mutational analysis of human tumours: a clinical platform to guide personalized cancer medicine. EMBO Mol Med. 2010;2:146–58.
31. Dias-Santagata D, Lennerz JK, Sadow PM, Frazier RP, Raju SG, Henry D, et al. Response to RET-specific therapy in RET fusion-positive anaplastic thyroid carcinoma. Thyroid. 2020. https://doi.org/10.1089/thy.2019.0477. [published online ahead of print, 2020 May 19].
32. Haugen BR, Alexander EK, Bible KC, Doherty GM, Mandel SJ, Nikiforov YE, et al. 2015 American Thyroid Association management guidelines for adult patients with thyroid nodules and differentiated thyroid cancer: the American Thyroid Association Guidelines Task Force on thyroid nodules and differentiated thyroid cancer. Thyroid. 2016;26:1–133.
33. Prasad ML, Vyas M, Horne MJ, Virk RK, Morotti R, Liu Z, et al. NTRK fusion oncogenes in pediatric papillary thyroid carcinoma in northeast United States. Cancer. 2016;122:1097–107.
34. Tallini G, Santoro M, Helie M, Carlomagno F, Salvatore G, Chiappetta G, et al. RET/PTC oncogene activation defines a subset of papillary thyroid carcinomas lacking evidence of progression to poorly differentiated or undifferentiated tumor phenotypes. Clin Cancer Res. 1998;4:287–94.
35. Adeniran AJ, Zhu Z, Gandhi M, Steward DL, Fidler JP, Giordano TJ, et al. Correlation between genetic alterations and microscopic features, clinical manifestations, and prognostic characteristics of thyroid papillary carcinomas. Am J Surg Pathol. 2006;30:216–22.
36. Pisarchik AV, Ermak G, Fomicheva V, Kartel NA, Figge J. The ret/PTC1 rearrangement is a common feature of Chernobyl-associated papillary thyroid carcinomas from Belarus. Thyroid. 1998;8:133–9.
37. Sisdelli L, Cordioli M, Vaisman F, Moraes L, Colozza-Gama GA, Alves PAG Jr., et al. AGK-BRAF is associated with distant

metastasis and younger age in pediatric papillary thyroid carcinoma. Pediatr Blood Cancer. 2019;66:e27707.
38. Musholt TJ, Musholt PB, Khaladj N, Schulz D, Scheumann GF, Klempnauer J. Prognostic significance of RET and NTRK1 rearrangements in sporadic papillary thyroid carcinoma. Surgery. 2000;128:984–93.
39. Kelly LM, Barila G, Liu P, Evdokimova VN, Trivedi S, Panebianco F, et al. Identification of the transforming STRN-ALK fusion as a potential therapeutic target in the aggressive forms of thyroid cancer. Proc Natl Acad Sci USA. 2014;111:4233–8.
40. Pérot G, Soubeyran I, Ribeiro A, Bonhomme B, Savagner F, Boutet-Bouzamondo N, et al. Identification of a recurrent STRN/ALK fusion in thyroid carcinomas. PLoS ONE. 2014;9:e87170.
41. Agrawal N, Akbani R, Aksoy B, Ally A, Arachchi H, Asa S, et al. Integrated genomic characterization of papillary thyroid carcinoma. Cell. 2014;159:676–90.
42. Liu SV, Macke LA, Colton BS, Imran SS, Christiansen J, Chow-Maneval E, et al. Response to entrectinib in differentiated thyroid cancer with a ROS1 fusion. JCO Precis Oncol. 2017;1:1–5.
43. Sheu SY, Schwertheim S, Worm K, Grabellus F, Schmid KW. Diffuse sclerosing variant of papillary thyroid carcinoma: lack of BRAF mutation but occurrence of RET/PTC rearrangements. Mod Pathol. 2007;20:779–87.
44. Joung JY, Kim TH, Jeong DJ, Park SM, Cho YY, Jang HW, et al. Diffuse sclerosing variant of papillary thyroid carcinoma: major genetic alterations and prognostic implications. Histopathology. 2016;69:45–53.
45. Acquaviva G, Visani M, Repaci A, Rhoden KJ, de Biase D, Pession A, et al. Molecular pathology of thyroid tumours of follicular cells: a review of genetic alterations and their clinicopathological relevance. Histopathology. 2018;72:6–31.
46. Grabenstetter A, Mohanty AS, Rana S, Zehir A, Brannon AR, D'Alfonso TM, et al. E-cadherin immunohistochemical expression in invasive lobular carcinoma of the breast: correlation with morphology and CDH1 somatic alterations. Hum Pathol. 2020; S0046-8177(20)30108-8. https://doi.org/10.1016/j.humpath.2020.06.002. [published online ahead of print, 2020 Jun 26].
47. Landa I, Ibrahimpasic T, Boucai L, Sinha R, Knauf JA, Shah RH, et al. Genomic and transcriptomic hallmarks of poorly differentiated and anaplastic thyroid cancers. J Clin Investig. 2016;126:1052–66.
48. Pozdeyev N, Gay LM, Sokol ES, Hartmaier R, Deaver KE, Davis S, et al. Genetic analysis of 779 advanced differentiated and anaplastic thyroid cancers. Clin Cancer Res. 2018;24:3059–68.
49. Xu B, Fuchs T, Dogan S, Landa I, Katabi N, Fagin JA, et al. Dissecting anaplastic thyroid carcinoma: a comprehensive clinical, histologic, immunophenotypic, and molecular study of 360 cases. Thyroid. 2020. https://doi.org/10.1089/thy.2020.0086. [published online ahead of print, 2020 May 8].
50. Zhou C, Zeng L, Zhang Y, Yang N. Responder of gefitinib plus crizotinib in osimertinib failure EGFR-mutant NSCLC-resistant with newly identified STRN-ALK by next-generation sequencing. J Thorac Oncol. 2019;14:e143–e4.
51. Yang Y, Qin SK, Zhu J, Wang R, Li YM, Xie ZY, et al. A rare STRN-ALK fusion in lung adenocarcinoma identified using next-generation sequencing-based circulating tumor DNA profiling exhibits excellent response to crizotinib. Mayo Clin Proc Innov Qual Outcomes. 2017;1:111–6.
52. Kron A, Alidousty C, Scheffler M, Merkelbach-Bruse S, Seidel D, Riedel R, et al. Impact of TP53 mutation status on systemic treatment outcome in ALK-rearranged non-small-cell lung cancer. Ann Oncol. 2018;29:2068–75.
53. Couëtoux du Tertre M, Marques M, Tremblay L, Bouchard N, Diaconescu R, Blais N, et al. Analysis of the genomic landscape in ALK+ NSCLC patients identifies novel aberrations associated with clinical outcomes. Mol Cancer Ther. 2019;18:1628–36.
54. Lin C, Shi X, Yang S, Zhao J, He Q, Jin Y, et al. Comparison of ALK detection by FISH, IHC and NGS to predict benefit from crizotinib in advanced non-small-cell lung cancer. Lung Cancer. 2019;131:62–8.
55. Pailler E, Faugeroux V, Oulhen M, Mezquita L, Laporte M, Honoré A, et al. Acquired resistance mutations to ALK inhibitors identified by single circulating tumor cell sequencing in ALK-rearranged non-small-cell lung cancer. Clin Cancer Res. 2019;25:6671–82.
56. Chang H, Sung JH, Moon SU, Kim HS, Kim JW, Lee JS. EGF induced RET inhibitor resistance in CCDC6-RET lung cancer cells. Yonsei Med J. 2017;58:9–18.
57. Nelson-Taylor SK, Le AT, Yoo M, Schubert L, Mishall KM, Doak A, et al. Resistance to RET-inhibition in RET-rearranged NSCLC is mediated by reactivation of RAS/MAPK signaling. Mol Cancer Ther. 2017;16:1623–33.
58. Sasaki T, Koivunen J, Ogino A, Yanagita M, Nikiforow S, Zheng W, et al. A novel ALK secondary mutation and EGFR signaling cause resistance to ALK kinase inhibitors. Cancer Res. 2011;71:6051–60.
59. Song A, Kim TM, Kim D-W, Kim S, Keam B, Lee S-H, et al. Molecular changes associated with acquired resistance to crizotinib in *ROS1*-rearranged non–small cell lung cancer. Clin Cancer Res. 2015;21:2379–87.
60. Stransky N, Cerami E, Schalm S, Kim JL, Lengauer C. The landscape of kinase fusions in cancer. Nat Commun. 2014;5:4846.
61. Ross JS, Wang K, Chmielecki J, Gay L, Johnson A, Chudnovsky J, et al. The distribution of BRAF gene fusions in solid tumors and response to targeted therapy. Int J Cancer. 2016;138:881–90.
62. Nikiforova MN, Hamilton RL. Molecular diagnostics of gliomas. Arch Pathol Lab Med. 2011;135:558–68.
63. Chmielecki J, Hutchinson KE, Frampton GM, Chalmers ZR, Johnson A, Shi C, et al. Comprehensive genomic profiling of pancreatic acinar cell carcinomas identifies recurrent RAF fusions and frequent inactivation of DNA repair genes. Cancer Discov. 2014;4:1398–405.
64. Johnson DB, Zhao F, Noel M, Riely GJ, Mitchell EP, Wright JJ, et al. Trametinib activity in patients with solid tumors and lymphomas harboring BRAF non-v600 mutations or fusions: results from NCI-MATCH (EAY131). Clin Cancer Res. 2020;26:1812–9.
65. Botton T, Yeh I, Nelson T, Vemula SS, Sparatta A, Garrido MC, et al. Recurrent BRAF kinase fusions in melanocytic tumors offer an opportunity for targeted therapy. Pigment Cell Melanoma Res. 2013;26:845–51.
66. Botton T, Talevich E, Mishra VK, Zhang T, Shain AH, Berquet C, et al. Genetic heterogeneity of BRAF fusion kinases in melanoma affects drug responses. Cell Rep. 2019;29:573–88.e7.
67. Ciampi R, Knauf JA, Kerler R, Gandhi M, Zhu Z, Nikiforova MN, et al. Oncogenic AKAP9-BRAF fusion is a novel mechanism of MAPK pathway activation in thyroid cancer. J Clin Investig. 2005;115:94–101.